

Drop splashing is independent of substrate wetting

Andrzej Latka,^{1, a)} Arnout M. P. Boelens,² Sidney R. Nagel,¹ and Juan J. de Pablo²

¹⁾*The James Franck Institute and Department of Physics, The University of Chicago, 929 E 57th Street, Chicago, Illinois 60637, USA*

²⁾*Institute for Molecular Engineering, The University of Chicago, 5801 South Ellis Avenue, Chicago, Illinois 60637, USA*

(Dated: August 29, 2018)

A liquid drop impacting a dry solid surface with sufficient kinetic energy will splash, breaking apart into numerous secondary droplets. This phenomenon shows many similarities to forced wetting, including the entrainment of air at the contact line. Because of these similarities and the fact that forced wetting has been shown to depend on the wetting properties of the surface, existing theories predict splashing to depend on wetting properties as well. However, using high-speed interference imaging we observe that at high capillary numbers wetting properties have no effect on splashing for various liquid-surface combinations. Additionally, by fully resolving the Navier-Stokes equations at length and time scales inaccessible to experiments, we find that the shape and motion of the air-liquid interface at the contact line at the edge of the droplet are independent of wettability. We use these findings to evaluate existing theories and to compare splashing with forced wetting.

I. INTRODUCTION

At first glance, one might suppose that the same physics should describe a solid plunging into a liquid and a liquid drop impacting a solid: both scenarios revolve around a liquid-gas-solid contact line that is forced to move at large velocities. In the former case, exceeding a critical contact line velocity leads to the destabilization of the contact line and the entrainment of gas bubbles in the liquid. This phenomenon, called dewetting¹ or wetting failure², is also observed in drop impact³. It has therefore been suggested that the onset of contact line instability can serve as an onset criterion for drop splashing^{4,5}. However, contrary to intuition, in this work we find that splashing is independent of the wetting properties of the surface⁶. This result helps us to further our understanding of the many processes that rely on splashing droplets, including erosion, coating, cleaning, cooling, high-throughput drug screening, and different printing technologies^{7,8}.

The wetting of a solid by a liquid depends on many parameters, including viscosity, surface tension, contact line velocity, impurities in the liquid, and roughness and heterogeneities of the substrate⁹. In addition, there is the complication that for a moving contact line the classical fluid-mechanics assumption of a no-slip condition on the wall breaks down¹⁰, and that due to strong local curvature at a contact line the observed contact angle is not necessarily the same as the microscopic contact angle¹¹. For real substrates, which show contact angle hysteresis due to surfaces roughness and chemical heterogeneity, the situation is even more complicated; while it is known from experiments that surface roughness can either enhance or reduce splashing depending on its characteristic length scale¹², in general its effect on wetting and contact

angle hysteresis is poorly understood⁹.

For smooth surfaces experiments on forced wetting have typically focused on the relationship between the velocity of the edge of the liquid/gas interface and the observed dynamic contact angle. Typically, in the steady state case when the contact angle is plotted as a function of the non-dimensionalized edge velocity, i.e. the capillary number, a single curve is found^{13,14}. For low capillary numbers and a completely wetting surface it has been experimentally well established¹⁵ that the contact line moves according to the Tanner-Voinov law^{16,17}. For partly wetting liquids with a sufficiently high viscosity the data can be described by a variation of the same law without the assumption of small slopes¹⁸. For forced wetting at larger capillary numbers the contact line eventually becomes unstable, and this is a topic of active research¹.

Models of forced wetting^{1,19} use the wetting properties of the surface as a boundary condition to determine the stability threshold for the contact line. Indeed, the wettability of the object that is plunged into a liquid has been found to have a strong influence on wetting failure²⁰. In contrast to recent conclusions based on simulations^{7,21}, we present experimental results which show that for rapidly moving contact lines, for a wide array of liquids, the surface wettability has negligible effect on splashing. We also describe simulations that are able to resolve contact line behavior at high resolution. These simulations reveal that the contact line motion previously associated with splashing on completely wetting surfaces²², is nearly identical for a completely non-wetting surface. Before dewetting, the rapidly moving contact line in both the wetting and the non-wetting case shows a microscopic contact angle of 180° . This suggests that the assumption of a fixed microscopic contact angle is inapplicable to contact lines that are forced to move at high speeds, as is the case in splashing, and challenges theories based on this assumption.

^{a)}Electronic mail: alatka@uchicago.edu

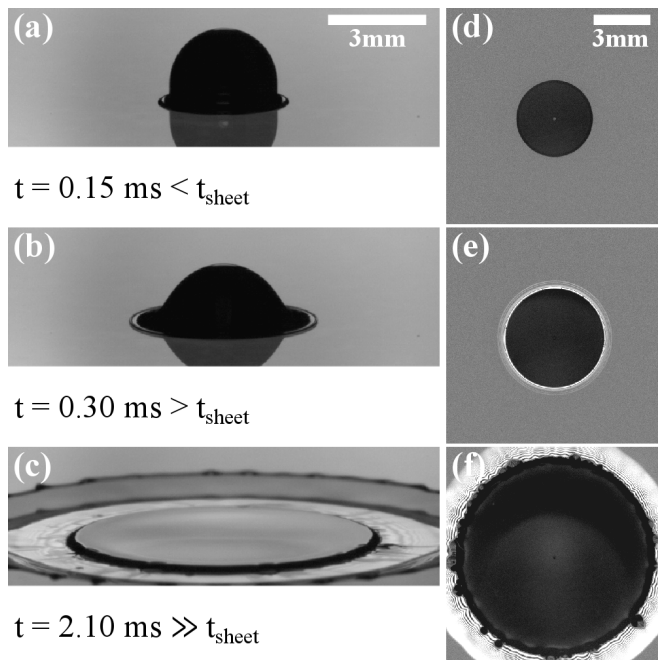


Figure 1. Successive images of a 9.4cP silicone oil drop of diameter 3.2 mm impacting a glass slide at 3.3 m/s at atmospheric pressure. Images (a) - (c) show the side view of the drop and its reflection, while (d) - (f) show the interference measurement from below at corresponding times. Initially, the drop spreads fully wetting the substrate in the form of a lamella. After time $t_{sheet} = 0.21\text{ms}$ an air gap appears between the liquid and solid, seen clearly as bright interference fringes (e,f), resulting in the creation of a thin liquid sheet (b,c) that extends from the thicker lamella.

II. METHODS

A. Experiments

The experiments were conducted with either silicone oil (PDMS, Clearco Products) of viscosity $\mu = 9.4$ and 32cP or a mixture of water and glycerol ($\mu = 32\text{cP}$). The drops with diameter $D = 3.3 \pm 0.1\text{mm}$ were produced at a nozzle with a syringe pump and were accelerated by gravity to an impact velocity of $V = 3.4 \pm 0.1\text{ms}^{-1}$. This resulted in the non-dimensional numbers and ratios shown in Tab. I. The silicone oil drops impacted glass slides (Fisherbrand Microscope Slides) that were left untreated to provide a completely wetting surface, with contact angle $\theta_0 = 0^\circ$, or glass slides covered with an oleophobic coating (Fussode Coat, $\theta_0 = 42 \pm 2^\circ$). Similarly, the water-glycerol drops impacted either clean glass ($\theta_0 = 36 \pm 3^\circ$), glass coated with indium tin oxide ($\theta_0 = 79 \pm 4^\circ$) or a hydrophobic coating (RainX, $\theta_0 = 90 \pm 3^\circ$). A wetting substrate was achieved for the water-glycerol by pre-wetting the glass slide with the same mixture. A liquid drop fully wets such a prepared slide ($\theta_0 = 0^\circ$), however the coating is thin enough not to change the splashing behavior. The changing of sub-

strates only affects the contact angle and does not change the spreading dynamics. Fig. 2 shows that drops spread at the same rate regardless of θ_0 . Air was used as the ambient gas, whose pressure P was controlled in a vacuum chamber ($5\text{kPa} \leq P \leq 101\text{kPa}$). Impacts were recorded with high-speed cameras (Vision Research) at rates up to 130 000 fps either from the side as in Fig. 1(a-c), or with interference imaging (d-f). The latter method measures the interference between light reflected from the bottom surface of the spreading liquid and the top surface of the substrate. Wherever the liquid is in contact with the substrate, there is no reflection of light from that surface and thus no light entering the camera. Wherever the two are separated, an interference pattern is created, as seen in Fig. 1(e-f). Since this method is particularly sensitive to the presence of the air gap, it allows us to measure precisely when the contact line begins to entrain air³.

A typical splash is presented in the left column of Fig. 1. Fig. 1(a) shows that a drop does not splash immediately. Instead the liquid spreads radially outward in the form of a lamella^{23,24}. The simultaneous interference image shows that the lamella fully wets the substrate. Beginning at time t_{sheet} after impact (where we define t_{sheet} as the time when the thin sheet first starts to appear at the front of the expanding lamella) one can observe an interference pattern at the liquid-air-solid contact line, as in Fig. 1(e), indicating the presence of a gas film that is of order a micron thick that separates the spreading liquid from the substrate. The time t_{sheet} is the start of the formation of a thin sheet of liquid^{3,23}, as can be seen in Fig. 1(b). The thin-sheet grows and ultimately breaks up into the secondary droplets that form the splash ($t = 2.1\text{ms}$, Fig. 1(c,f)).

The thin-sheet creation time depends on a number of parameters²³. Most importantly, t_{sheet} is delayed as the ambient gas pressure is reduced. However, if the pressure is decreased below a threshold pressure P_{sheet} , instead of being further delayed, the thin sheet will fail to appear and the splash will have been completely suppressed²⁵⁻²⁷. We quantify the effect of wetting on splashing by measuring the dependence of both t_{sheet} and P_{sheet} on the surface properties.

B. Simulations

To be able to examine the contact line in more detail, we simulate the breakup of a splashing drop using a finite volume implementation of the volume of fluid method²⁸. The VOF approach evolves around the definition of a phase parameter α with the following properties:

$$\alpha = \begin{cases} 0 & \text{in gas phase} \\ (0, 1) & \text{on interface} \\ 1 & \text{in liquid phase} \end{cases} \quad (1)$$

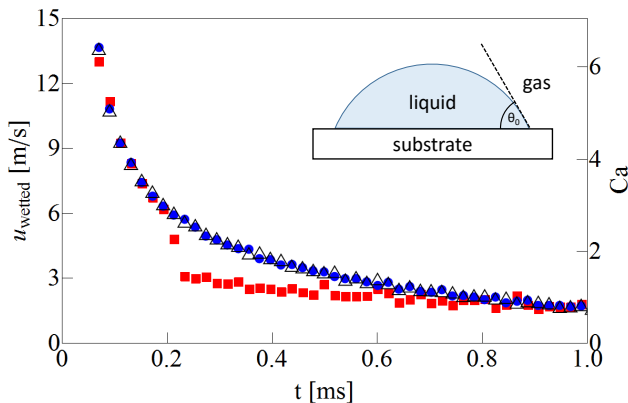


Figure 2. Speed (left axis) and capillary number (right axis) of the advancing liquid-solid contact line as a function of time after impact of a 9.4cP silicone oil drop on glass ($\theta_0 = 0^\circ$, \blacktriangle) or glass coated with an oleophobic layer ($\theta_0 = 42^\circ$, \triangle). Splashing was suppressed by reducing the pressure to $P = 30\text{kPa} < P_{\text{sheet}}$. The presence of a coating does not influence spreading speed. At atmospheric pressure (\blacksquare) air entrainment begins at $t_{\text{sheet}} = 0.21\text{ms}$ after which the contact line slows. The diagram shows that Young’s angle θ_0 , at which a stationary gas-liquid interface meets the substrate, is measured in the liquid phase.

The evolution of α is calculated using the following transport equation:

$$\frac{\partial \alpha}{\partial t} + \nabla \cdot (\alpha \vec{v}) + \nabla \cdot (\alpha(1 - \alpha) \vec{v}_{lg}) = 0, \quad (2)$$

where \vec{v} is the phase averaged velocity, and \vec{v}_{lg} is a velocity field suitable to compress the interface. This equation is equivalent to a material derivative, but rewritten to minimize numerical diffusion²⁹.

The phase parameter is used to calculate the phase averaged density, ρ , velocity, \vec{v} , and viscosity, μ , which are used in the momentum balance:

$$\frac{\partial \rho \vec{v}}{\partial t} + \nabla \cdot (\rho \vec{v} \otimes \vec{v}) = -\nabla p + \nabla \cdot (\mu \nabla \vec{v}) + \rho \vec{g} - \vec{f}, \quad (3)$$

and the continuity equation:

$$\nabla \cdot \vec{v} = 0. \quad (4)$$

In the above equations t is time, p is pressure, g is gravity, \vec{f} is any body force, like the surface tension force, and \otimes is the dyadic product. To complete the VOF model, an expression is needed to calculate the surface tension force \vec{f}_{st} , and a model is needed for the contact line. The surface tension force is calculated using the expression³⁰:

$$\vec{f}_{\text{st}} = \sigma_{\text{st}} \kappa \nabla \alpha \quad (5)$$

where σ_{st} is the surface tension coefficient, and κ is the curvature of the interface.

The effect of varying the Young’s angle θ_0 from 0° to 180° is calculated directly through the generalized Navier

boundary condition at the impact wall^{31,32}. With this boundary condition the dynamic contact angle θ is allowed to vary freely, but a restoring line-tension force is applied at the contact line whenever the dynamic angle deviates from θ_0 . This restoring force is an additional source term in the Navier-Stokes equations, and has the following form:

$$\vec{f}_{\text{lt}} = -\frac{\sigma}{h} \cos \theta_0 \nabla_{2D} \alpha \quad (6)$$

In the above equation σ is the surface tension coefficient, h is the height of the local grid cell, and $\nabla_{2D} \alpha$ is the gradient of α on the wall. This force is applied on the liquid-gas interface in the first grid cells adjacent to the wall and is balanced by the surface tension force when θ is equal to θ_0 . Away from the contact line the used implementation of the generalized Navier boundary condition reduces to the Navier-slip boundary condition. Using this slip boundary condition gives a good approximation for the thin film behavior at the wall^{33,34}. Because the model used can accommodate only one value for the slip length, a value of $\lambda = 1\text{nm}$ is chosen to be able to describe the contact line accurately. However, in practice the effective slip length is on the order of the mesh size of 10nm ³⁵. This results in the gas film potentially closing faster in our simulations than if the slip length were truly 1nm .

The simulations are performed for ethanol in air using the VOF solver of the OpenFOAM Finite Volume toolbox³⁶ at up to 10nm resolution at the wall³⁷. More information on the boundary conditions at the contact line can be found in Ref. 38. More information on the equations, initial conditions, and a comparison with experiments can be found in Ref. 22. In this paper it is shown that the scaling of the gas film height as function of impact velocity is consistent with theory and experiments, and multiple experimental observations are reproduced, including the formation of the central air bubble, liquid sheet formation, and contact line instability²².

To reduce memory requirements, we consider an ethanol ($\mu = 1.1\text{cP}$) droplet with a diameter of $300\mu\text{m}$, as opposed to the 3mm more viscous droplets used in the experiments. This results in the non-dimensional numbers shown in Tab. I. As can be seen in this table the non-dimensional numbers for the whole droplet are quite different between the experiments and simulations. However, the focus of this work is on the capillary number at the contact line/edge of the droplet, which, as is shown below, is of the same order between simulations and experiments. In addition, as the splashing threshold has been shown to scale across a wide range of parameters^{5,24,39}, comparisons with experiments should not be compromised.

Table I. An overview of the non-dimensional numbers and ratios of liquid and gas properties under conditions of our experiments.

	Re	We	ρ_l/ρ_g	ν_l/ν_g
Silicone oil (9.4 cP)	1106	1759	0.6852	927
Silicone oil (32 cP)	335	1762	2.262	956
Water & glycerol (32 cP)	418	686	1.825	1191
Ethanol	986	264	0.1028	789

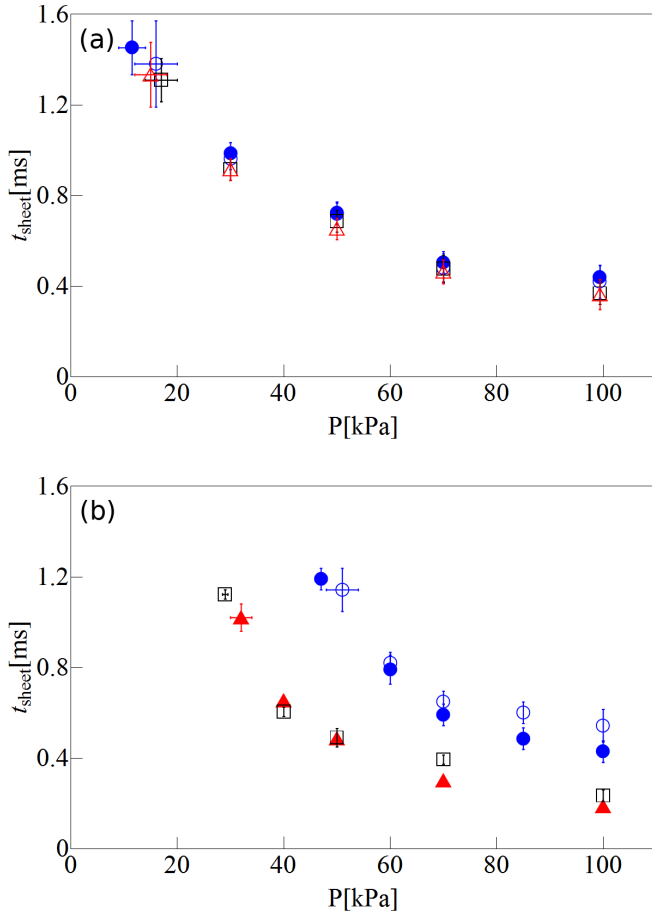


Figure 3. Time of thin-sheet creation vs. ambient gas pressure for droplet impacts on glass slides with different wetting angles. Image (a) shows the impact of 32cP water-glycerol drops on glass slides with $\theta_0 = 0^\circ$ (●), 36° (○), 79° (□), and 90° (△). t_{sheet} is independent of wetting. Image (b) shows the impact of 9.4cP silicone oil drops on glass slides with $\theta_0 = 0^\circ$ (●) and 42° (○), and of 32cP silicone oil drops on glass slides with θ_0 of 0° (▲) and 42° (□). The small differences in t_{sheet} with wetting properties are within error.

III. RESULTS

A. Experiments

Varying the surface wettability does not affect t_{sheet} , as shown for water-glycerol drops in Fig. 3 (a). Notably, the onset of thin-sheet creation is surprisingly indepen-

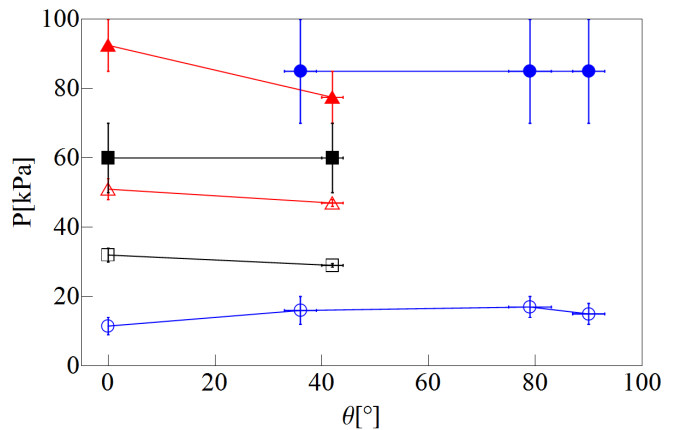


Figure 4. Threshold pressure for drop breakup P_{splash} (filled symbols) and thin-sheet creation P_{sheet} (empty symbols) vs. contact angle: 32cP water-glycerol (●), 32cP silicone oil (▲) and 9.4cP silicone oil (■). Thin sheets created at $P_{\text{sheet}} < P < P_{\text{splash}}$ will not break apart. Neither threshold is affected by surface wettability.

dent of changes in surface properties. Not only does a hydrophobic coating fail to change t_{sheet} , but even coating the glass slide with a thin layer of water-glycerol yields the same result. Similarly, no noticeable effect of wetting can be seen for silicone oil drops in Fig. 3 (b), where the substrate was changed from fully wetting with $\theta_0 = 0^\circ$ to partially wetting with $\theta_0 = 42^\circ$.

Fig. 4 compares the threshold pressure for the different substrates. As the ambient pressure is decreased, t_{sheet} is delayed and the resulting thin-sheet is diminished. Consequently, below a pressure P_{splash} , the thin-sheet is too small to break apart into secondary droplets and splashing is suppressed. If the ambient pressure is further decreased below P_{sheet} , the thin-sheet is never formed. We find that both P_{sheet} and P_{splash} are independent of θ_0 . This result is similar to the velocity threshold in Ref. 20, which was also independent of θ_0 for $\theta_0 < 90^\circ$.

B. Simulations

The simulation results shown in Fig. 5 compare the shape of the air-liquid interface for wetting and non-wetting surfaces at different stages of impact. The interface has a thickness of about 20nm, which is two times the highest resolution of the simulations. To facilitate comparisons with experiments, velocity is non-dimensionalized as the capillary number $\text{Ca} \equiv \frac{\mu V}{\sigma}$. At all times for which $\text{Ca} \geq 1$ the interface is the same on both surfaces and, within the resolution of the simulations, the microscopic contact angle in both cases is 180° . The observed gas film is about 20nm thick.

Only for times at which $\text{Ca} < 1$ do the interfaces begin to look different; the contact angle on the non-wetting surface remains 180° , while the contact angle on the wetting surface decreases and would converge to its equilib-

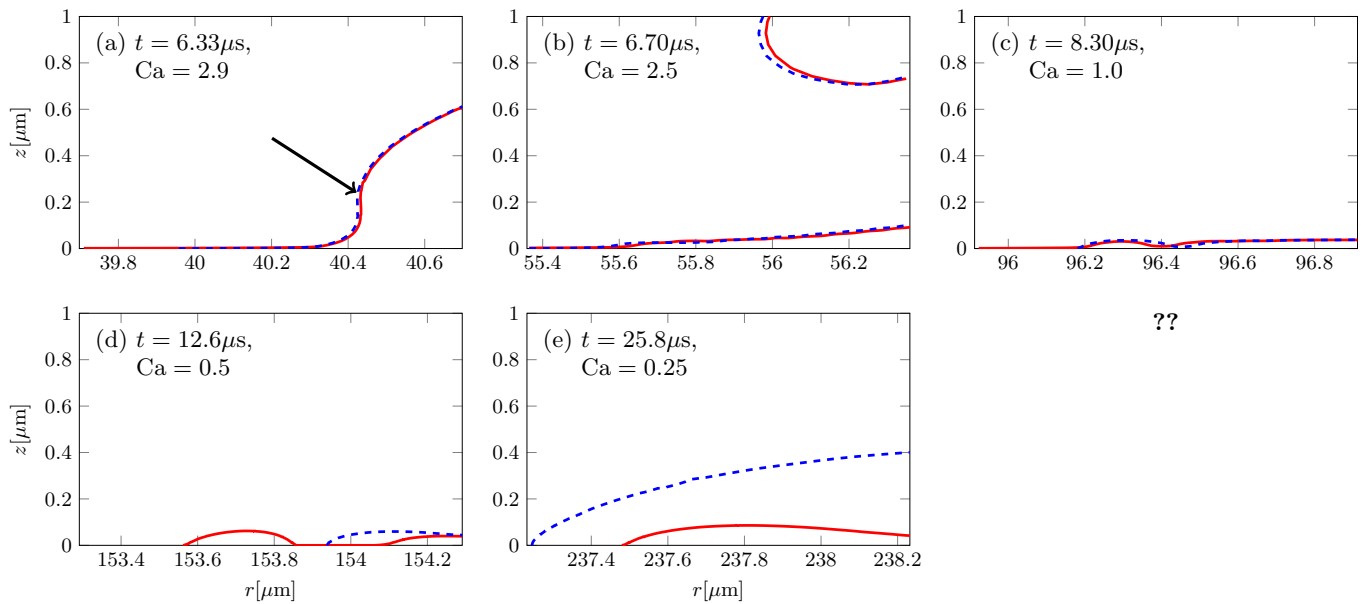


Figure 5. Time series of the droplet interface showing the contact-line evolution for a simulated droplet with the parameters of ethanol at atmospheric pressure for $\theta_0 = 0^\circ$ (wetting) and $\theta_0 = 180^\circ$ (non-wetting). The vertical axis shows height above the surface and the horizontal axis shows the radial distance from the point of impact. (a) The moment a cusp (indicated by the black arrow) can first be observed in the interface. This is the onset of lamella formation. (b) Immediately after t_{sheet} . A gas film is present under the liquid sheet and the interface approaches the surface at a 180° angle. (c) The transition from the $\text{Ca} > 1$, high-speed contact line regime to the $\text{Ca} < 1$, low-speed regime. (d) As explained in section III B, this frame shows a touch-down event of the interface on the non-wetting surface: a gas bubble is entrained behind the contact line. (e) The gas film forming on the wetting surface at low speeds is thicker than the gas film on the non-wetting surface.

rium Young's angle, $\theta_0 = 0^\circ$, if the simulation were to run long enough until the drop is stationary.

A consequence of the lower θ in the wetting case at low Ca is a thicker gas film at the contact line compared to the non-wetting surface, as can be observed most clearly in Fig. 5 (e). Independent of the wetting properties, the gas film thickness is greatest when the air-liquid interface becomes parallel to the substrate (cf. Figs. 5 (c-e)). The lower θ at the contact line of a wetting substrate requires a longer arc length to satisfy this condition, which results in a thicker gas film. Additionally, a greater separation between the liquid sheet and the substrate stabilizes the contact line. At early times, the gas film in front of the contact line periodically collapses and the liquid touches down on the substrate, entraining air bubbles (Fig. 5 (d)). The contact line on the non-wetting surface never stabilizes and bubbles are entrained throughout the simulation. In contrast, these touch-down events are no longer observed at late times on the wetting surface.

A quantitative description of the differences in contact line behavior for splashing on wetting versus non-wetting surfaces is provided in Fig. 6 (a) by plotting the microscopic contact angle as function of the capillary number for wetting and non-wetting surfaces. In agreement with Fig. 5, for $\text{Ca} > 1$ both wetting and non-wetting surfaces show the same contact angle of 180° . When the contact line slows to $\text{Ca} < 1$ the non-wetting surface continues to exhibit $\theta = 180^\circ$, while the wetting surface exhibits a

contact angle that decreases with Ca .

The change of behavior at $\text{Ca} \approx 1$ is shown via the standard deviation of the microscopic contact angle in Fig. 6 (b). For the non-wetting surface $\theta = 180^\circ$ at all times, therefore the fluctuations are small and independent of the capillary number. For the wetting surface at large capillary numbers the fluctuations are also small, however shortly before $\text{Ca} = 1$ they begin to grow dramatically as $\text{Ca} \rightarrow 1$. This behavior is reminiscent of a phase transition, where fluctuations increase around the critical point. Taking this analogy further, this suggests that not only does the contact angle change for $\text{Ca} < 1$, but, more importantly, the flow enters a different flow regime. Note that this result is unrelated to the aforementioned touch-down events, which are instabilities of the apparent contact angle.

Fig. 7 shows the horizontal and vertical liquid sheet ejection velocities, measured at the rim of the liquid sheet. Fig. 5 shows that a cusp forms in the interface at the same time for both wetting and non-wetting surfaces. Consequently, one can expect the liquid sheet, which forms promptly after the cusp can be detected, to be ejected at the same velocity. This is confirmed in Fig. 7, which demonstrates that the liquid sheets are ejected at the same angle, independent of wetting properties. As time progresses the figures show that the trajectories of the liquid sheet are nearly identical for the wetting and non-wetting case.

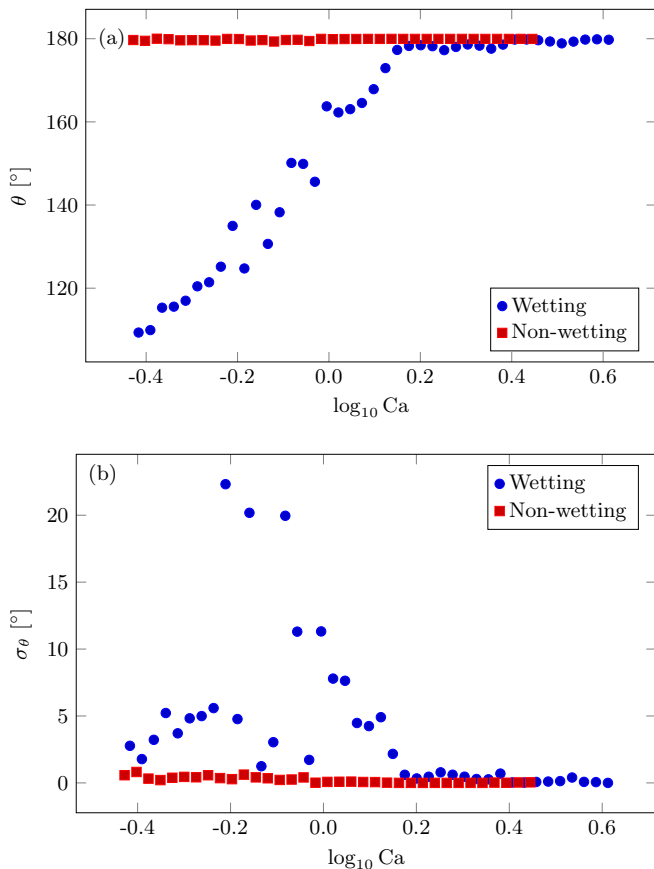


Figure 6. Image (a) shows the average mean contact angle as a function of the capillary number for a simulated droplet with the parameters of ethanol at atmospheric pressure. For wetting surfaces a transition can be observed for $Ca \approx 1$ where the microscopic angle goes from $\theta < 180^\circ$ to $\theta = 180^\circ$. For the non-wetting surface the microscopic angle stays constant. Image (b) shows the standard deviation of the contact angle as a function of the capillary number for a simulated droplet with the parameters of ethanol at atmospheric pressure. For wetting surfaces, the contact line regime change around $Ca \approx 1$ causes the fluctuations of the microscopic contact angle to increase significantly. This increase in fluctuations is not observed for non-wetting surfaces.

IV. DISCUSSION

The key to understanding the unusual contact line behavior in splashing is in contrasting it with that of slow-moving contact lines. A stationary contact line will approach a homogeneous surface at an angle θ_0 that is determined purely by wetting properties. If the contact line is forced to move, as in the classic case of a solid being plunged into a liquid bath, the shape of the interface will be determined by both the capillary number, which describes the balance between surface tension and viscous forces, and gravity¹. In addition, the assumption is made that the contact line is moving slowly enough that the microscopic contact angle is independent of the capillary number and is equal to Young's angle θ_0 , which

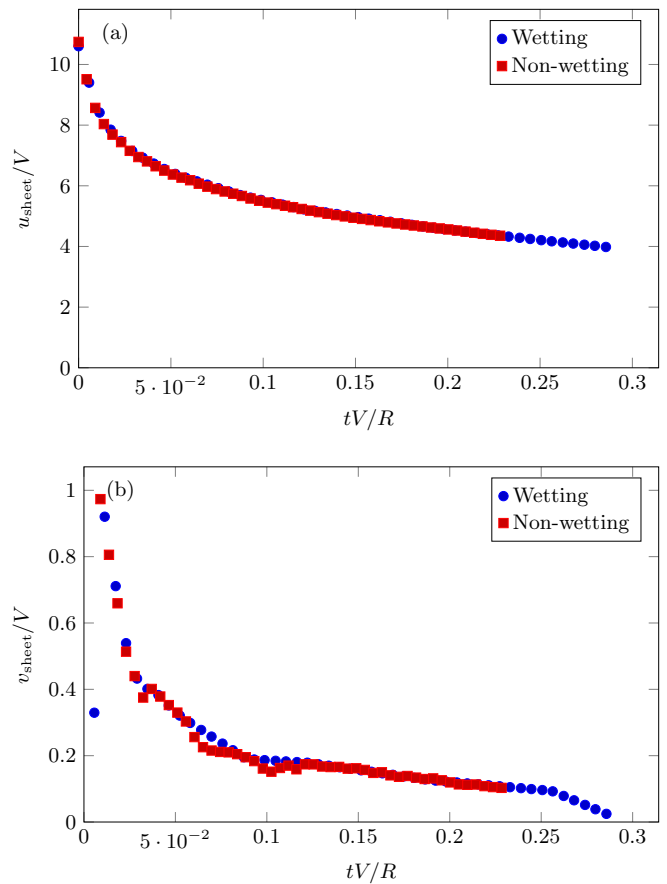


Figure 7. Image (a) shows the horizontal liquid sheet ejection velocity as a function of time for a simulated droplet with the parameters of ethanol at atmospheric pressure. Velocities and time are made non-dimensional with the impact velocity V and droplet radius R . Image (b) shows the vertical liquid sheet ejection velocity as a function of time for a simulated droplet with the parameters of ethanol at atmospheric pressure. Velocities and time are made non-dimensional with the impact velocity V and droplet radius R . Wetting and non-wetting surfaces show the same behavior.

now serves as a boundary condition at the surface. For advancing contact lines this results in a critical capillary number at which this boundary condition cannot be satisfied^{1,40}. Consequently, theory predicts that above this critical capillary number wetting failure will be observed in the form of air bubble entrainment at the contact line. Additionally, it is predicted that the critical capillary number depends on the wetting properties of the surface⁵.

The splash of the liquid drop occurs in multiple stages. Shortly before impact, the bottom surface of the drop is deformed by the rising gas pressure in the decreasing gap between the liquid and solid^{41,42}. When the liquid makes contact with the substrate, the air directly beneath the drop is trapped into a small bubble confined to the center of the deposited liquid^{43,44}, while the liquid begins spreading radially outward in the form of an axisymmet-

ric lamella⁴⁵. Our simulations of lamella creation, described in more detail in Ref. 22, are consistent with the predictions made in Refs. 41, 45, and 5. The contact line moves fastest immediately after impact, and proceeds to rapidly decelerate as shown in Fig. 2. Fig. 2 further reveals that at the moment of thin-sheet formation the capillary number (on the right axis) of the contact line is in the unstable regime: at atmospheric pressure $t_{\text{sheet}} = 0.21\text{ms}$ with $\text{Ca}(t_{\text{sheet}}) = 2.9$. Therefore at all times between impact and sheet creation $\text{Ca} > 2.9$.

The time of thin-sheet creation, t_{sheet} , varies with multiple parameters, most importantly with the ambient gas pressure. However, in all cases we find that thin-sheet creation occurs when $\text{Ca}(t_{\text{sheet}}) \gtrsim 1$. Indeed, for the points shown in Fig. 3 (a) a thin-sheet is created with $1.2 < \text{Ca}(t_{\text{sheet}}) < 7.5$, for the 32 cP drops in Fig. 3 (b) $1.6 < \text{Ca}(t_{\text{sheet}}) < 5.1$, and for the 9.4 cP drops in Fig. 3 (b) $0.7 < \text{Ca}(t_{\text{sheet}}) < 3.0$. A wide range of parameters was investigated in Ref. 46. Impact velocity, drop size, surface tension, density, surface tension, viscosity of both the liquid and the gas, and the gas molecular weight were varied. It was invariably found that splashing can occur only when the contact line is moving at a large Ca.

The high resolution of our simulations allow us to determine that at such high Ca the contact line is advancing via a "rolling" motion²². In both the wetting, $\theta_0 = 0^\circ$, and non-wetting, $\theta_0 = 180^\circ$, case, an ultra-thin air gap extends underneath the drop, as can be seen in Fig. 5(a-c). This is equivalent to a dynamic contact angle $\theta = 180^\circ$ that is independent of the static wetting properties. In other words, splashing is independent of wetting, because splashing occurs at large Ca, at which the static wetting properties do not influence the shape of the contact line. Although we can identify this air film in simulations, in experiments we are only able to detect the thicker gas film that is present after t_{sheet} . However, the ultra-thin air film was already experimentally observed by Kolinski et al. via total internal reflection measurements⁴⁷ and is consistent with the analysis in Ref. 4.

The presence of this air film can have a profound effect on drop impact. If the substrate is sufficiently smooth and the impact velocity sufficiently low, the ultra-thin air persists underneath the drop and isolates it from substrate, so that a drop can rebound from a wetting substrate, as if it were super-hydrophobic⁴⁸. However, drops splash at much higher impact velocities. In this case, Kolinski et al. observed that the air film behind the advancing contact line was closed within several microseconds, and attributed the effect to interactions between the liquid and solid^{47,49,50}. This is consistent with the observation that while splashing, which originates directly at the contact line, is independent of the wetting properties for both contact angles smaller than 90° and larger than 90° ⁶, the slower dynamics following splashing are still determined by the static contact angle. For example, the maximum spreading diameter of an impact-droplet does depend on the properties of the solid⁵¹⁻⁵³.

We emphasize that the wetting independence of splashing is a direct result of contact line dynamics. While our simulations agree with Ref. 54 with respect to the presence of a boundary layer and also find a characteristic "rolling" motion of the contact line, we find, in agreement with Ref. 47, that these phenomena result from the rapid motion of the contact line.

The behavior of the splashing contact line at high Ca provides a means of testing splashing theories, such as the model recently proposed by Riboux and Gordillo^{5,55} or by Liu et al.⁵⁶. In the Riboux and Gordillo model the wetting properties influence the calculated lubrication lift force on the edge of the spreading liquid. As the liquid edge rises, its rim increases in size due to surface tension and, consequently, the bottom surface of the rim is forced downward. Depending on which of these effects dominates, the lamella either continues moving upward and eventually breaks apart to form a splash, or rewets the substrate, which prevents splashing. The lubrication force calculated is dependent strongly on the shape of the advancing contact line set by the microscopic contact angle, (c.f. footnote [35] in Ref. 5). Consequently, the theory predicts the splashing threshold to strongly depend on the wetting properties of the substrate; this is inconsistent with the results presented here from experiments and simulations. Furthermore, this model predicts that splashing occurs at time $t_{e,crit}$ after impact, calculated from Eqn. 1 in Ref. 5. In contrast, we find that in all cases $t_{\text{sheet}} \gg t_{e,crit}$ ^{3,23,24}. The disparity is most evident for drops of higher viscosity near threshold pressure, for which t_{sheet} is largest. For these drops, $t_{e,crit}$, which does not depend on pressure, is smaller than t_{sheet} by several orders of magnitude. Together, these results suggest that the microscopic basis of this and similar theories should be revisited. In contrast, Liu et al. propose that splashing is caused by the Kelvin-Helmholtz instability in the air film that was observed in Ref. 47 and in our simulations. While our results are not a direct test of this model, they are consistent with its implicit contact angle independence.

V. CONCLUSION

Splashing arises from the interaction of three phases: the liquid drop, the solid substrate, and the ambient gas. It is therefore surprising that the most basic measure of this interaction, the contact angle θ_0 , does not influence the outcome of drop impact for the impact parameters we have investigated. Our experiments show that both the time of the splash, as well as the splashing thresholds are independent of θ_0 . Direct numerical simulations allow us to probe the advancing liquid-gas interface at nm length scales and show that the shape of this interface is the same for $\theta_0 = 0^\circ$ and $\theta_0 = 180^\circ$.

Splashing occurs when the liquid is spreading rapidly across the substrate, at capillary numbers $\text{Ca} \geq 1$. In this regime, both experiments⁴⁷ and simulations²² sug-

gest that the advancing contact line spreads over a short-lived thin film of air. Understanding the dynamics of this air film, both its rapid growth at t_{sheet} (where we define t_{sheet} as the time when the thin sheet first starts to appear at the front of the expanding lamella) that leads to splashing, and how t_{sheet} is set by ambient pressure, is crucial to forming an accurate model of splashing.

ACKNOWLEDGMENTS

This work was supported by the University of Chicago Materials Research and Engineering Center (MRSEC) through grant DMR-1420709 and by the NSF grant DMR-1404841. The VOF simulation method for splashing employed here was developed with support from the Multi-University Research Initiative (MURI) program - Office of Naval Research (MURI) - N00014-11-1-0690.

REFERENCES

- ¹A. Marchand, T. S. Chan, J. H. Snoeijer, and B. Andreotti, “Air entrainment by contact lines of a solid plate plunged into a viscous fluid,” *Physical Review Letters* **108**, 204501 (2012).
- ²E. Vandre, M. S. Carvalho, and S. Kumar, “Delaying the onset of dynamic wetting failure through meniscus confinement,” *Journal of Fluid Mechanics* **707**, 496–520 (2012).
- ³M. M. Driscoll and S. R. Nagel, “Ultrafast interference imaging of air in splashing dynamics,” *Physical Review Letters* **107**, 154502 (2011).
- ⁴M. Rein and J.-P. Delplanque, “The role of air entrainment on the outcome of drop impact on a solid surface,” *Acta Mechanica* **201**, 105–118 (2008).
- ⁵G. Riboux and J. M. Gordillo, “Experiments of Drops Impacting a Smooth Solid Surface: A Model of the Critical Impact Speed for Drop Splashing,” *Physical Review Letters* **113**, 024507 (2014).
- ⁶T. C. de Goede, K. G. de Bruin, and D. Bonn, “Splashing of impacting drops,” (2017), arXiv:1701.02504.
- ⁷C. Josserand and S. Thoroddsen, “Drop impact on a solid surface,” *Annual Review of Fluid Mechanics* **48**, 365–391 (2016).
- ⁸A. K. Price, A. B. MacConnell, and B. M. Paegel, “Microfluidic Bead Suspension Hopper,” *Anal. Chem.* **86**, 5039–5044 (2014).
- ⁹D. Bonn, J. Eggers, J. Indekeu, J. Meunier, and E. Rolley, “Wetting and spreading,” *Reviews of modern physics* **81**, 739–805 (2009).
- ¹⁰C. Huh and L. Scriven, “Hydrodynamic model of steady movement of a solid/liquid/fluid contact line,” *Journal of Colloid and Interface Science* **35**, 85–101 (1971).
- ¹¹E. Dussan, “On the spreading of liquids on solid surfaces: static and dynamic contact lines,” *Annual Review of Fluid Mechanics* **11**, 371–400 (1979).
- ¹²A. Latka, A. Strandburg-Peshkin, M. M. Driscoll, C. S. Stevens, and S. R. Nagel, “Creation of prompt and thin-sheet splashing by varying surface roughness or increasing air pressure,” *Physical Review Letters* **109**, 054501 (2012).
- ¹³R. L. Hoffman, “A study of the advancing interface. I. Interface shape in liquid–gas systems,” *Journal of Colloid and Interface Science* **50**, 228–241 (1975).
- ¹⁴J. Ralston, M. Popescu, and R. Sedev, “Dynamics of wetting from an experimental point of view,” *Annual Review of Materials Research* **38**, 23–43 (2008).
- ¹⁵J. Berg, *Wettability*, Vol. 49 (CRC, 1993).
- ¹⁶O. Voinov, “Hydrodynamics of wetting,” *Fluid Dynamics* **11**, 714–721 (1976).
- ¹⁷L. Tanner, “The spreading of silicone oil drops on horizontal surfaces,” *Journal of Physics D: Applied Physics* **12**, 1473–1483 (1979).
- ¹⁸R. Cox, “The dynamics of the spreading of liquids on a solid surface. Part 1. Viscous flow,” *Journal of Fluid Mechanics* **168**, 169–194 (1986).
- ¹⁹J. H. Snoeijer, B. Andreotti, G. Delon, M. Fermigier, *et al.*, “Relaxation of a dewetting contact line. Part 1. A full-scale hydrodynamic calculation,” *Journal of Fluid Mechanics* **579**, 63–83 (2007).
- ²⁰C. Duez, C. Ybert, C. Clanet, and L. Bocquet, “Making a splash with water repellency,” *Nature Physics* **3**, 180–183 (2007).
- ²¹K. Yokoi, “Numerical studies of droplet splashing on a dry surface: triggering a splash with the dynamic contact angle,” *Soft Matter* **7**, 5120–5123 (2011).
- ²²A. M. P. Boelens, A. Latka, and J. J. de Pablo, “Observation of the pressure effect in simulations of droplets splashing on a dry surface,” (2016), arXiv:1601.02134.
- ²³M. M. Driscoll, C. S. Stevens, and S. R. Nagel, “Thin film formation during splashing of viscous liquids,” *Physical Review E* **82**, 036302 (2010).
- ²⁴C. S. Stevens, A. Latka, and S. R. Nagel, “Comparison of splashing in high- and low-viscosity liquids,” *Physical Review E* **89**, 063006 (2014).
- ²⁵L. Xu, W. W. Zhang, and S. R. Nagel, “Drop splashing on a dry smooth surface,” *Physical Review Letters* **94**, 184505 (2005).
- ²⁶L. Xu, L. Barcos, and S. R. Nagel, “Splashing of liquids: Interplay of surface roughness with surrounding gas,” *Physical Review E* **76**, 066311 (2007).
- ²⁷L. Xu, “Liquid drop splashing on smooth, rough, and textured surfaces,” *Physical Review E* **75**, 056316 (2007).
- ²⁸C. Hirt and B. Nichols, “Volume of fluid (VOF) method for the dynamics of free boundaries,” *Journal of Computational Physics* **39**, 201–225 (1981).
- ²⁹H. Rusche, *Computational Fluid Dynamics of Dispersed Two-Phase Flows at High Phase Fractions*, Ph.D. thesis, Imperial College (2002).
- ³⁰J. Brackbill, D. Kothe, and C. Zemach, “A continuum method for modeling surface tension,” *Journal of Computational Physics* **100**, 335–354 (1992).
- ³¹T. Qian, X.-P. Wang, and P. Sheng, “Molecular scale contact line hydrodynamics of immiscible flows,” *Physical Review E* **68**, 016306 (2003).
- ³²J.-F. Gerbeau and T. Lelievre, “Generalized Navier boundary condition and geometric conservation law for surface tension,” *Computer Methods in Applied Mechanics and Engineering* **198**, 644–656 (2009).
- ³³E. Lauga, M. Brenner, and H. Stone, “Microfluidics: the no-slip boundary condition,” in *Springer handbook of experimental fluid mechanics* (Springer, 2007) pp. 1219–1240.
- ³⁴J. E. Sprittles, “Kinetic effects in dynamic wetting,” *Physical Review Letters* **118**, 114502 (2017).
- ³⁵D. Jacqmin, “Contact-line dynamics of a diffuse fluid interface,” *Journal of Fluid Mechanics* **402**, 57–88 (2000).
- ³⁶OpenCFD Ltd, “OpenFOAM (Version 2.1.0) [Computer software],” (2011).
- ³⁷The pressure field is solved using the Preconditioned Conjugate Gradient solver (PCG) with the Geometric Agglomerated Algebraic Multigrid (GAMG) pre-solver. The tolerance was set to 10^8 to ensure convergence. For divergence terms a Gauss Upwind Scheme was used. OpenFOAM regulates the time step size through the Courant number, which was set to 0.1 to ensure a small time step and numerical stability.
- ³⁸A. M. P. Boelens and J. J. de Pablo, “Generalized navier boundary condition for a volume of fluid approach using a finite-volume method,” (2016), arXiv:1604.07880.
- ³⁹C. S. Stevens, “Scaling of the splash threshold for low-viscosity fluids,” *Europhysics Letters* **106**, 24001 (2014), 1403.3145.
- ⁴⁰H. Benkreira and M. Khan, “Air entrainment in dip coating under reduced air pressures,” *Chemical Engineering Science* **63**,

- 448–459 (2008).
- ⁴¹S. Mandre, M. Mani, and M. P. Brenner, “Precursors to splashing of liquid droplets on a solid surface,” *Physical Review Letters* **102**, 134502 (2009).
- ⁴²S. Mandre and M. P. Brenner, “The mechanism of a splash on a dry solid surface,” *Journal of Fluid Mechanics* **690**, 148–172 (2012).
- ⁴³S. Chandra and C. Avedisian, “On the collision of a droplet with a solid surface,” (*The Royal Society*, 1991) pp. 13–41.
- ⁴⁴S. T. Thoroddsen, K. Takehara, and T. Etoh, “Bubble entrapment through topological change,” *Physics of Fluids* (1994-present) **22**, 051701 (2010).
- ⁴⁵A. Mongruel, V. Daru, F. Feuillebois, and S. Tabakova, “Early post-impact time dynamics of viscous drops onto a solid dry surface,” *Physics of Fluids* **21**, 032101 (2009).
- ⁴⁶A. Latka, “Thin-sheet creation and threshold pressures in drop splashing,” *Soft Matter* **13**, 740–747 (2017).
- ⁴⁷J. M. Kolinski, S. M. Rubinstein, S. Mandre, M. P. Brenner, D. A. Weitz, and L. Mahadevan, “Skating on a film of air: drops impacting on a surface,” *Physical Review Letters* **108**, 074503 (2012).
- ⁴⁸J. Kolinski, L. Mahadevan, and S. Rubinstein, “Drops can bounce from perfectly hydrophilic surfaces,” *EPL (Europhysics Letters)* **108**, 24001 (2014).
- ⁴⁹F. B. Wyart and J. Daillant, “Drying of solids wetted by thin liquid films,” *Canadian Journal of Physics* **68**, 1084–1088 (1990).
- ⁵⁰S. G. Yiantsios and B. G. Higgins, “Rupture of thin films: Non-linear stability analysis,” *Journal of Colloid and Interface Science* **147**, 341–350 (1991).
- ⁵¹S. Wildeman, C. W. Visser, C. Sun, and D. Lohse, “On the spreading of impacting drops,” *Journal of Fluid Mechanics* **805**, 636–655 (2016).
- ⁵²C. Antonini, A. Amirfazli, and M. Marengo, “Drop impact and wettability: From hydrophilic to superhydrophobic surfaces,” *Physics of fluids* **24**, 102104 (2012).
- ⁵³Š. Šikalo, H.-D. Wilhelm, I. Roisman, S. Jakirlić, and C. Tropea, “Dynamic contact angle of spreading droplets: Experiments and simulations,” *Physics of Fluids* **17**, 062103 (2005).
- ⁵⁴J. Philippi, P.-Y. Lagrée, and A. Antkowiak, “Drop impact on a solid surface: short-time self-similarity,” *Journal of Fluid Mechanics* **795**, 96–135 (2016).
- ⁵⁵G. Riboux and J. M. Gordillo, “The diameters and velocities of the droplets ejected after splashing,” *Journal of Fluid Mechanics* **772**, 630–648 (2015).
- ⁵⁶Y. Liu, P. Tan, and L. Xu, “Kelvin–Helmholtz instability in an ultrathin air film causes drop splashing on smooth surfaces,” *Proceedings of the National Academy of Sciences* **112**, 3280–3284 (2015).